ELECTRONIC AND GEOMETRIC STRUCTURE OF CO ON Ni(110): EXPERIMENT AND THEORY

H. KUHLENBECK, M. NEUMANN

Fachbereich Physik, Universität Osnabrück, D-4500 Osnabrück, Fed. Rep. of Germany

and

H.-J. FREUND

Institut für Physikalische und Theoretische Chemie der Universität Erlangen – Nürnberg, Egerlandstrasse 3, D-8520 Erlangen, Fed. Rep. of Germany

Chemisorption of CO on Ni(110) results at saturation in a well ordered (2×1)p2mg structure observed in LEED. The strong lateral interaction between the CO molecules leads to the formation of a two-dimensional band structure, which has been investigated in great detail by angle resolved photoelectron spectroscopy using monochromatized light from the storage ring BESSY at Berlin. Due to the low symmetry and the existence of two CO molecules in the unit cell eight valence bands have been observed, namely the $4\sigma^+$, $4\sigma^-$, $5\sigma^+$, $5\sigma^-$, $1\pi_x^+$, $1\pi_x^-$, $1\pi_y^+$ and $1\pi_y^-$ bands. The experimentally determined band structure can be well reproduced by tight binding calculations of an unsupported CO overlayer of p2mg symmetry, if the interaction with the substrate is included so as to account for 4σ–5σ mixing upon chemisorption as well as for the 5σ–1π hybridization. Certain deviations between experiment and theory allow us to deduce information about the possible influence of indirect intermolecular interactions. The dispersion of the $1\pi_x$ bands turned out to be very sensitive to the tilt angle of the CO molecules. An inclination of $17 \pm 2°$ from the normal along the [001] direction alternating to both sides has been evaluated, consistent with a structure of p2mg symmetry rather than p1g1 symmetry.

1. Introduction

Recently, Behm et al. [1] have investigated adlayer geometry and structural effects in the CO/Ni(110) system for various coverages using low energy electron diffraction (LEED), temperature programmed desorption spectroscopy (TDS) and work function measurements. They conclude from their study together with results from the literature that the CO molecules are adsorbed on the Ni rows in [1$\bar{1}$0] direction and that the separation of the CO molecules is dominated by short range CO–CO repulsion rather than by Ni–CO interaction. At saturation coverage ($\theta = 1.0$) below 250 K a particularly interesting structure exists. In this case the high density of the adlayer

results in a lateral tilt of the CO. Behm et al. [1] interpret the (2 × 1) LEED pattern as a p2mg superstructure. From LEED measurements itself it is difficult to decide whether the observed LEED structure corresponds to a p2mg or a p1g1 structure. The molecular tilt direction is *parallel* to the [001] direction for the p2mg structure and it is *not* parallel to [001] for the p1g1 structure. Thus, the difference between the two structures is the existence of an additional mirror plane in p2mg, which is detectable by angle resolved photoemission. Very recent angle resolved electron stimulated desorption measurements for CO/Ni(110) by Riedl and Menzel [2] show unequivocally the existence of a mirror plane along [001]. Nevertheless, the published results are contradictory for CO adsorption on Pt(110) [3–5]. Hofmann et al. [4] suggested a p1g1 structure of $\theta = 1.0$ coverage, whereas Rieger et al. [3] showed later using angle resolved photoelectron spectroscopy with polarized light that there must be an extra mirror plane in the system CO/Pt(110). The latter authors suggest a p2mg structure for the saturation coverage of CO on Pt(110).

In the present study we report results of extensive angle resolved photoemission measurements using synchrotron and laboratory source radiation on the system CO/Ni(110) at saturation coverage ($\theta = 1.0$).

Using a combination of experimental techniques and theoretical calculations it is our objective to answer the following three questions:

(i) Does CO interaction with a Ni(110) surface yield the same situation as CO interaction with Pt(110); although the nearest neighbour distance is considerably smaller for Ni as compared to Pt?

(ii) Is the magnitude of dispersion (E versus $k_{\parallel}$) of the adsorbate levels for a tilted CO molecule consistent with estimates gained from several previous studies of CO adsorbate level dispersion, i.e. on hexagonal (111) surfaces, where CO is bound perpendicular to the surface?

(iii) Can the observed CO adsorbate level dispersion be reasonably predicted by a band structure calculation of a two-dimensional CO layer? (Note, that the (110) surface has the pronounced advantage of allowing only for one type of CO domain structure). Furthermore, if this is possible, does the band dispersion allow us to estimate the tilt angle for the CO–metal bond.

We proceed by first outlining the experimental procedure and the results. Secondly we summarize the theoretical procedure together with the results gained to interpret the experimental observations. Thirdly, we discuss experimental and theoretical results of the present study with respect to literature data. Finally, a synopsis of the present study is presented.

2. Experimental procedure and results

The experiments were performed in two magnetically shielded ultra high vacuum systems (VG, ADES 400) containing facilities for low energy electron

diffraction (LEED), Auger electron spectroscopy (AES), residual gas analysis with a quadrupole mass spectrometer and angle resolved photoelectron spectroscopy (ARPES). The electron analyser is rotatable in two orthogonal planes and electrons are collected within an acceptance angle of $\pm 1.5°$. The resolution in energy was typically 100 meV. Excitation of photoelectrons with polarized UV light was achieved in one system by a capillary discharge lamp with a three-mirror polarizer, whereas the other system was attached to a torroidal grating monochromator (TGM) at the storage ring BESSY in Berlin. The base pressure in both systems was below 10^{-8} Pa.

The Ni(110) crystal was spotwelded between two tungsten wires which were spotwelded to tungsten rods mounted on a specimen sample manipulator. With liquid nitrogen the crystal could be cooled to 80 K. Heating was possible either directly or by electron impact onto the reverse side of the crystal. The surface was cleaned by argon ion bombardment. After annealing the cleanliness was checked with AES, and surface order and overlayer geometry were established by LEED.

Adsorption of CO at temperatures below 200 K results at saturation in a well ordered $(2 \times 1)p2mg$ structure corresponding to a coverage of $\theta = 1$. This structure is shown in fig. 1. The structural information has been obtained from different previous investigations [6–9,12]. From high resolution electron energy loss measurements (HREELS) [6–9] we know that only one specific adsorption site is occupied and all the CO molecules are bridge-bonded at saturation coverage. In thermal desorption spectroscopy (TDS) [1,2,10] a second desorption peak appears at coverages above $\theta = 0.8$, indicating that strong repulsive interaction starts at coverages above $\theta = 0.8$. Indeed, at coverages above $\theta = 0.8$ adjacent adsorption sites along the [1$\bar{1}$0] nickel rows must be occupied by the CO molecules. To avoid the strong intermolecular interaction, the CO molecules form zig-zag chains along the [1$\bar{1}$0] direction. At saturation coverage, $\theta = 1.0$, the axis of all CO molecules are tilted alternating to either sides of the [1$\bar{1}$0] Ni rows. The tilt angle will be determined in this work by ARPES and was independently determined by electron stimulated desorption (ESD) [2]. In LEED a (2×1) pattern is observed [1,11]. Due to the formation of the zig-zag chains glide line symmetry is achieved which leads to missing spots $(n/2,0)$ in the LEED pattern [11]. Possible notations are $(2 \times 1)p1g1$ or $(2 \times 1)p2mg$. By simple kinematic LEED investigations these two structures cannot be differentiated. The additional mirror plane in the p2mg structure can be determined in ARPES or ESD [2]. The ordering of the overlayer leads to extremely sharp extra spots. Note that there is only one domain and band mapping can be done perfectly along all directions without the common problem of the superposition of Brillouin zones of all of the existing domains.

Fig. 2 shows photoelectron spectra in normal emission of the clean and CO covered Ni(110) surface excited with unpolarized He I light (21.2 eV). Binding

Geometric structure of Ni(110)/CO(2×1)p2mg

Unit cell
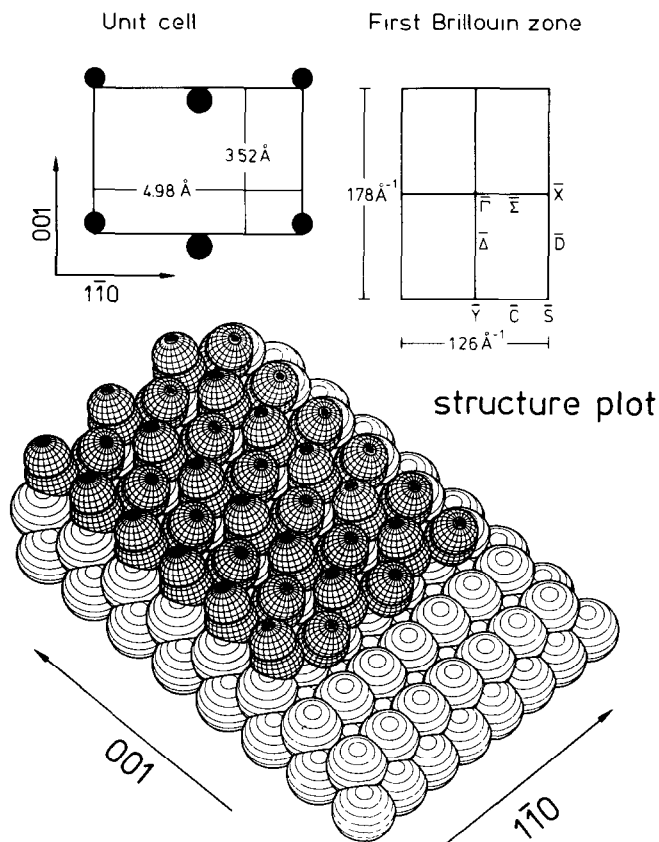
First Brillouin zone

structure plot

Fig. 1. Structural information for the system CO(2×1)p2mg/Ni(110). Upper left panel: size of the unit cell in real space with molecular positions schematically indicated. Upper right panel: size, points, and lines of high symmetry within the Brillouin zone. Lower panel: Structure plot based on LEED, EELS, ESD, and the present PES data for the p2mg structure.

energies are referenced to the Fermi level. Structure close to the Fermi level corresponds to photoemission from the nickel d-bands, which is strongly attenuated after adsorption of CO. Extra structures in the binding energy range of 1 to 3 eV are attributed either to surface umklapp processes or to bonding states of the CO molecule. These effects will be discussed in a separate paper [12]. Extra structures in the binding energy range of 5 to 11 eV are due to emission from energy bands derived from the CO 1π, 5σ and 4σ molecular ion states. There is no structure observed in the spectrum of the clean Ni(110) surface in this range. Emission from the nickel satellite at 6 eV
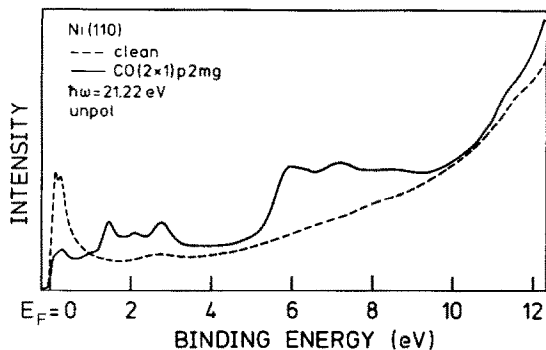
Fig. 2. Photoemission spectra of the clean and CO covered Ni(110) surface in normal emission using a He I source with unpolarized light. Energies are referenced to the Fermi level.

binding energy is very weak and does not interfere with the CO induced extra emission. Using higher photon energies (around $\hbar\omega = 65$ eV) the satellite becomes more intense [13]. Obviously the spectrum contains more than two or three CO induced structures typically seen in photoelectron spectra of adsorbed CO. As the symmetry of the adsorbed CO molecules is only twofold, the 1π level, which is degenerate in the gas phase, is split into a $1\pi_x$ and a $1\pi_y$ state. In addition, all the states $1\pi_x$, $1\pi_y$, 5σ and 4σ are split into symmetric and antisymmetric states, as there are two CO molecules in the unit cell. From this we expect eight bands, which actually were determined (see below). For the full determination of the band structure, it was necessary to collect many photoelectron spectra under different experimental conditions: (i) using polarized light the symmetry of the energy bands can be determined, (ii) taking spectra under different polar angles the determination of the dispersion of the two-dimensional bands is possible and (iii) varying the photon energy the relative intensities of the transitions change and thus a more accurate determination of binding energies of overlapping peaks is obtainable. Relative intensities change also by variation of the polar angle.

   In fig. 3 normal emission spectra from the valence bands of adsorbed carbon monoxide are shown in more detail. The spectra have been excited with polarized light from a gas discharge lamp. The different polarizations of the light are denoted by x, y and z. Here z-polarization corresponds to p-polarization with the electric field vector E predominantly perpendicular to the surface ($E \parallel [110]$) and s-polarization corresponds to x- and y-polarization with the E vector parallel to the surface. As the symmetry at $\bar{\Gamma}$ (normal emission) is only twofold, we expect different spectra for x-polarization ($E \parallel [1\bar{1}0]$ and y-polarization ($E \parallel [001]$). Spectra excited with He II ($\hbar\omega = 40.8$ eV) radiation are shown in the upper part of fig. 3. Emission around 11 eV is originating from the 4σ derived bands whereas emission from the 5σ and 1π derived bands appears from 6 to 9 eV. There is clear evidence for the existence
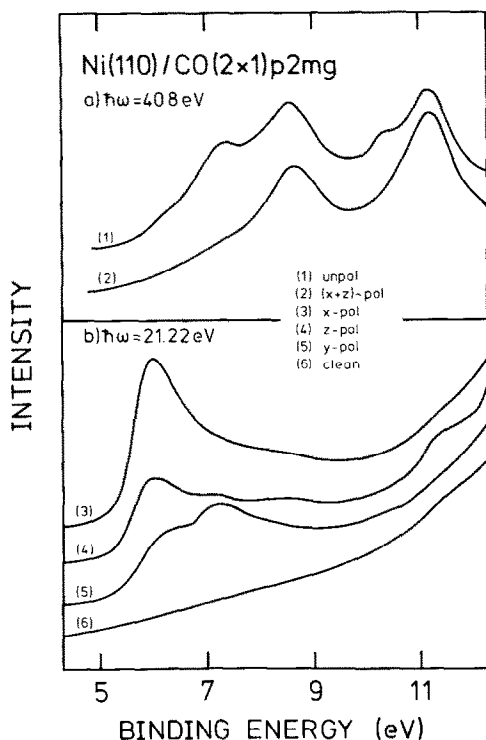
Fig. 3. Photoemission spectra in normal emission of the CO (2×1)p2mg structure excited with polarized light from a He resonance lamp. Energies are referenced to the Fermi level.

of two peaks around 11 eV which are attributed to a symmetric $4\sigma^+$ and an antisymmetric $4\sigma^-$ band. Comparing spectrum (1) and (2) additional structures appear in spectrum (1) which are obviously excited with y-polarized light. The prominent peaks in spectrum (2) arise from the $4\sigma^+$ and $5\sigma^+$ bands excited by z-polarized light. The additional structures in spectrum (1), therefore, can be attributed to $4\sigma^-$, $5\sigma^-$ and $1\pi_y^+$. In the lower part of fig. 3 spectra excited with polarized He I ($\hbar\omega = 21.22$ eV) light are presented. Caused by the enhancement of the 1π cross section at low photon energies [14] the strong emission in spectrum (3) arises from the $1\pi_x^+$ band. In spectra (3) to (5) emission from the 5σ and the 1π derived CO levels contribute due to their close energetic proximity. The strong intensity variations as a function of polarization x, y and z demonstrate quite clearly that it is important to collect data with all three polarizations to obtain full information on the symmetries of the valence bands of carbon monoxide. Spectrum (6) was taken from the clean Ni(110) surface. There is no structure seen in the spectrum except a tiny final state peak at 11.5 eV, which does not interfere with the CO-induced structures.
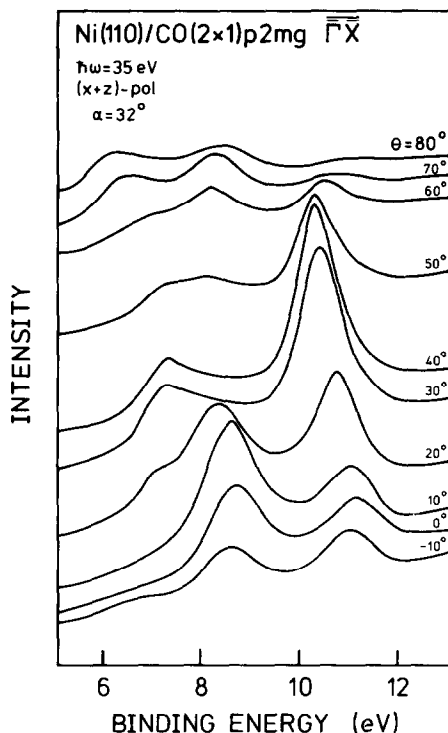
Fig. 4. Series of photoemission spectra taken at various polar angles θ in the $\overline{\Gamma X}$ azimuth excited with monochromatized synchrotron radiation ($\hbar\omega = 35$ eV). α is the angle of incidence of the light. Energies are referenced to the Fermi level.

Fig 4 shows a set of photoemission spectra obtained for various polar angles illustrating the dispersion of the 4σ and $5\sigma/1\pi$ bands. The data were collected with p-polarized light with a photon energy of $\hbar\omega = 35$ eV, where emission of the σ-orbitals is strongest [15]. The angle of incidence of the light was 32°. The momentum parallel to the surface of the collected electrons is pointing along the [1$\bar{1}$0] direction which corresponds to the $\overline{\Gamma X}$ line of the surface Brillouin zone. As the nearest neighbour distance of the investigated adsorbate system is very small, we observe large dispersion effects, namely 0.8 eV for the 4σ derived bands. Dispersion of the 5σ bands is also clearly seen. Going from $\theta = 20°$ to 30° we observe a sudden shift in the 5σ-peak position. This shift is attributed to a 5σ–1π hybridization as will be discussed in the course of the paper. Emission from the 1π bands is relatively weak at low polar angles and becomes more pronounced at higher polar angles [15]. Many more spectra have been collected to get a full description of the band structure. Although there are eight bands in an energy range of only 5 eV the dispersion of all bands could be observed by variation of polarization and
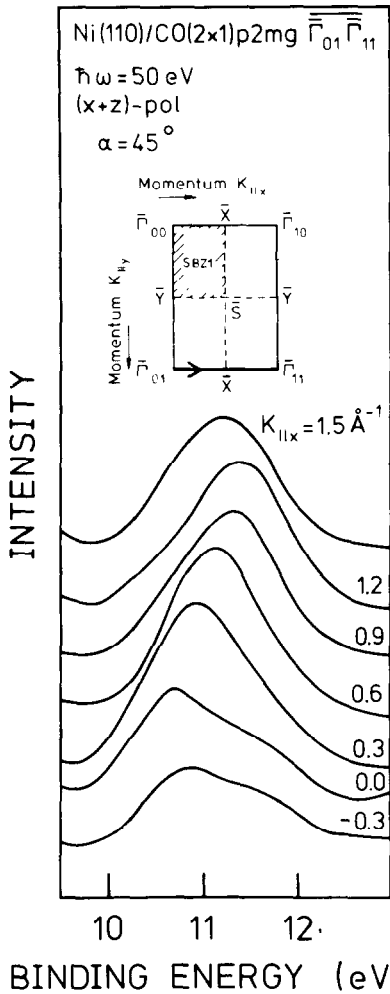
Fig. 5. Series of photoemission spectra along $\overline{\Gamma}_{01}\overline{X}\overline{\Gamma}_{11}$ taken by simultaneous variation of the polar and azimuthal angles. Monochromatized synchrotron radiation of $\hbar\omega = 50$ eV was used. Energies are referenced to the Fermi level.

energy of the incident light. There is no problem of summing intensities of differently oriented domains. Since there is only one single domain, we can collect data from any direction in the two-dimensional reciprocal space. As an example (fig. 5) we present data from a symmetry line $\overline{\Gamma}_{01}\overline{X}\overline{\Gamma}_{11}$ (see inset of fig. 5) in a higher surface Brillouin zone. The appropriate momentum in x and y direction parallel to the surface was obtained by a simultaneous variation of the polar and azimuthal angles. The spectra have been excited with p-polarized

light ($\hbar\omega = 50$ eV). There is again clear evidence that there are two 4σ derived bands. At the $\overline{X}$ point these bands are degenerate ($K_{\parallel x} = 0.63$ Å^{-1}). At the $\overline{Y}$ point a spliting of the 4σ derived band of 0.3 eV was observed in measurements not shown in fig. 5.

3. Theoretical procedure and results

We have carried out tight-binding calculations [16], assuming nearest and next nearest neighbour interactions with ab initio [17] and semi-empirical CNDO-type [18] (where CNDO means complete neglect of differential overlap) wavefunctions to determine the intermolecular interaction parameters. Details of the method have been given by Greuter et al. [19,20].

The basis functions to calculate the bands are the molecular orbitals. We assume an unsupported two-dimensional CO overlayer. In order to partially account for interaction of the CO molecules with the substrate we adopted the following procedure: We have calculated self-consistently a linear NiCO cluster [21], then "cut off" the CO from the metal and renormalized the CO wavefunctions. The renormalized wavefunctions are then used as basis functions. This procedure has several advantages, the main one is that through interaction with the metal the CO 5σ level is stabilized to be energetically close to the 1π level thus allowing for 5σ–1π hybridization [19], as was shown for CO/Co(0001) [19] in various adlayer geometries. Also, it allows for the necessary flexibility to describe the mixing of 5σ and 4σ levels. A consequence of this mixing is that for a given CO–CO spacing the 4σ interaction increases, while the 5σ interaction decreases. The calculated band widths follow this trend when the renormalized molecular wavefunctions instead of those of isolated CO are used. We have calculated the band structure of a CO overlayer in p2mg symmetry as a function of the tilt angle γ, γ is the angle between the surface normal and the CO–metal bond, which was assumed to be linear. A bent metal–CO bond has not been explicitly considered.

Fig. 1 shows a structure model based on LEED [1,11] and EELS [6–9] as well as the associated Brillouin zone results. Fig. 6 shows the complete band structure for this structure assuming a tilt angle $\gamma = 17°$. This is the band structure that will be compared with the experimental data in section 4. In this context we shall explain the determination of γ.

At this point let us consider the character of the calculated energy bands with respect to symmetry properties, band hybridization and associated two-dimensional wavefunctions at the points of highest symmetry. Clearly, the p2mg structure cannot be described by a primitive unit cell containing one molecule. As is indicated in the upper panels of fig. 1 there are two molecules per unit cell. For a description of the band structure the wavefunctions of a
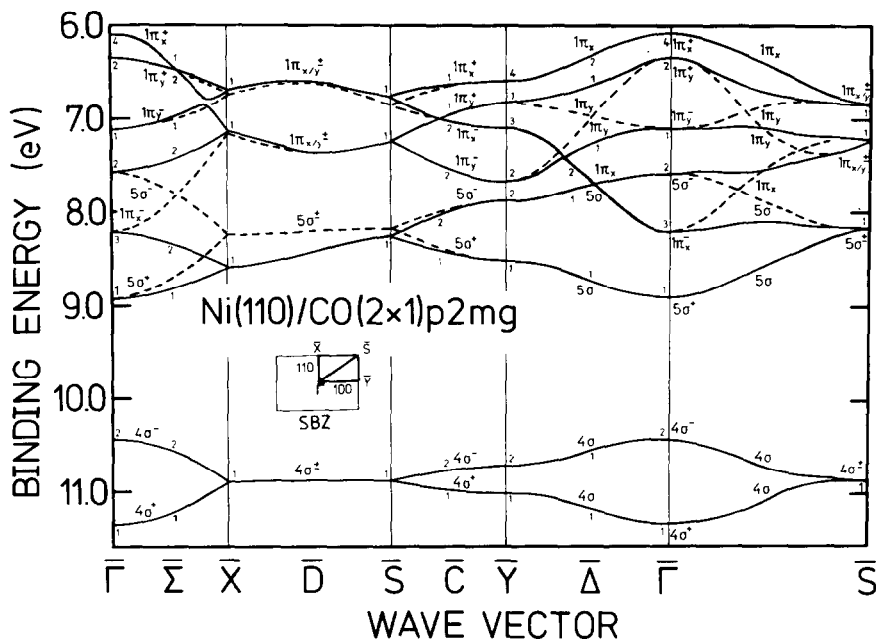
Fig. 6. Calculated bandstructure of a CO (2×1)p2mg overlayer with a molecular tilt angle of $\gamma = 17°$. For details see text.

single molecule are therefore not a proper basis. However, linear combinations

$\chi_1 = c_1 |CO_I\rangle + c_2 |CO_{II}\rangle$ symmetric

$\chi_2 = c_1 |CO_I\rangle - c_2 |CO_{II}\rangle$ asymmetric

of molecular CO wavefunctions located at the positions of the two molecules allow one to construct two-dimensional adlayer wavefunctions that transform according to p2mg symmetry and which give rise to bands (E versus $k_{\parallel}$) easy to label properly by their irreducible representation at the points of high symmetry. Fig. 7 schematically shows two-dimensional adlayer wavefunctions at $\bar{\Gamma}$, $\bar{X}$, and $\bar{Y}$ based on σ molecular wavefunctions (fig. 7a) and on π molecular wavefunctions (figs. 7b and 7c). The unit cell is indicated. χ_1 and χ_2 are plotted.

Consider fig. 7a to represent the 4σ orbitals of CO. Unlike the case of one molecule per unit cell leading to a single band per non-degenerate molecular orbital (MO) in the Brillouin zone, we have two bands in the present case, namely, one associated with the bonding, the other one with the antibonding combination of molecular orbitals. In the band structure the bands are labelled $+$ and $-$, respectively. At $\bar{\Gamma}$ the splitting into two bands is about 0.92 eV, caused by the strong lateral interaction. In the bonding combination
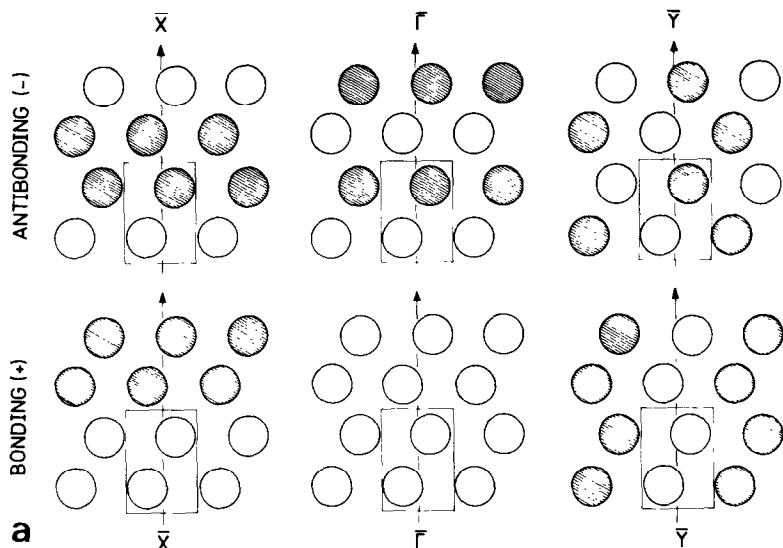
Fig. 7a. Schematic representation of a two-dimensional, periodic wavefunction of σ symmetry at high symmetry points of a (2×1)p2mg structure. Bonding and antibonding refers to the character of interaction within the unit cell. $+$ and $-$ refers to the phase relation among unit cells.
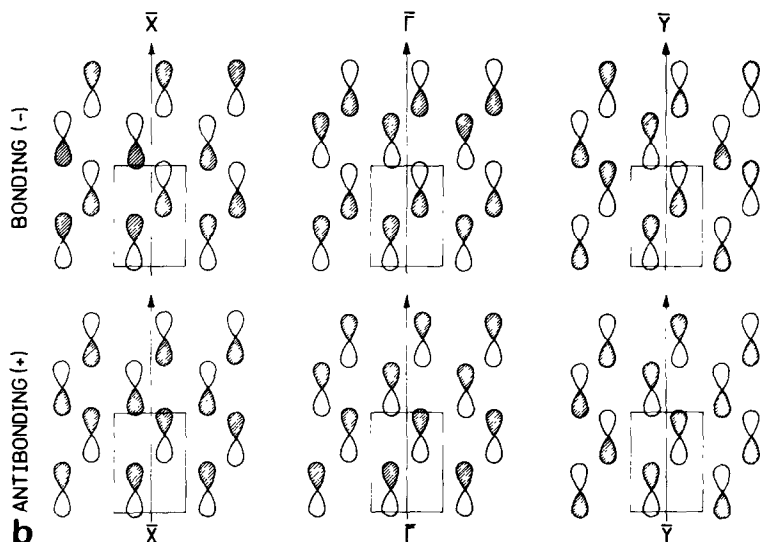

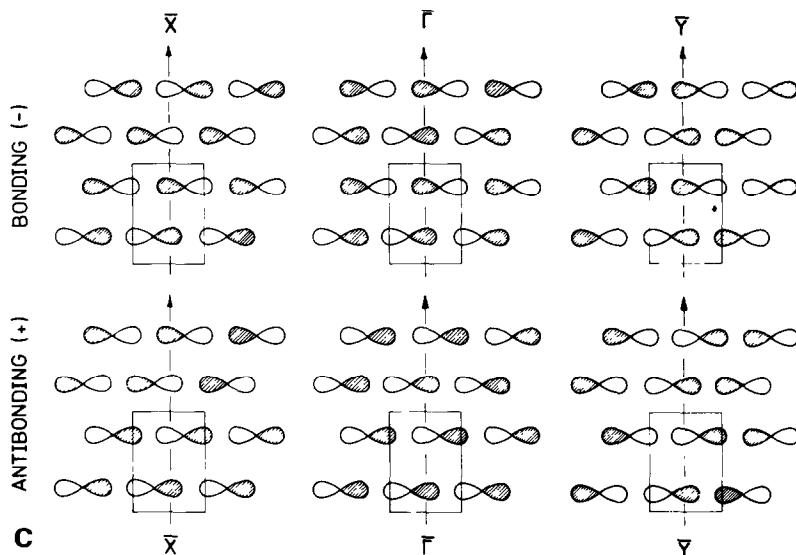Fig. 7b. As fig. 7a for π_x symmetry.

C

Fig. 7c. As fig. 7a for π_y symmetry.

all MOs have the same phase, i.e. the two-dimensional wavefunction is strongly bonding which leads to a stabilization on a binding energy scale compared to a laterally non-interacting adsorbate. The antibonding combination at $\bar{\Gamma}$ is antibonding with respect to the direction of the glide plane [1$\bar{1}$0] but bonding with respect to the [001] direction. The interaction is stronger along the closed packed [1$\bar{1}$0] direction thus leading to a net destabilization on a binding energy scale. The absolute amount of the splitting depends on the details of the intermolecular interaction matrix elements as they are used within the band-structure calculation. If we follow the bands in k-space along $\bar{\Gamma}$–$\bar{X}$ (the $\bar{\Sigma}$ direction), the + band increases, while the – band decreases in energy until they are degenerate at $\bar{X}$. Fig. 7a allows us to visualize the situation: At $\bar{X}$ the phase between unit cells has changed sign. Consequently, for the bonding combination this yields a two-dimensional wavefunction with phase changes only between double rows in [001] direction. For the antibonding combination the same wavefunction results which is evident from fig. 7a, causing the bands to become degenerate. In fact the bands have to be degenerate on the entire line $\bar{X}$–$\bar{S}$, i.e. the line perpendicular to the glide plane, as was shown by Hund [22]. Clearly, the wavefunction plots indicate that the energy position of the band at $\bar{X}$ has to be intermediate between the energies at $\bar{\Gamma}$ since there is increasing antibonding character for the bonding combination while there is loss of antibonding character for the antibonding combination. Along the $\bar{S}$–$\bar{Y}$ line, on the other hand, there is no symmetry restriction

for band degeneracy as shown in fig. 6. Again, the two-dimensional schematic wavefunctions indicate the reason: The phase change in this case occurs, unlike the former situation, perpendicular to the glide plane, leading to zig-zag chains which have internal bonding, towards the neighbouring chain, however, antibonding character. The wavefunctions and thus the bands are non-degenerate energetically, since the spatial separation between sites of equal phase is larger for the − than for the + band. The splitting at $\overline{Y}$ is 0.3 eV, which should be compared with 0.92 eV at $\overline{\Gamma}$. In order to specify the character of the wavefunctions (fig. 7a) within the band structure plot (fig. 6) the irreducible representations of the wavefunctions are indicated as Arabic numbers according to the convention proposed by Litvin [23,24]. (Note that instead of writing $\overline{\Gamma}_1$ or $\overline{Y}_4$ we only give the subscript at the particular high symmetry point or line.)

Next, we consider the region of the band structure at lower binding energies, namely, the region of the 5σ and 1π molecular orbitals. Due to the low symmetry of the overlayer 5σ and 1π derived adlayer bands are allowed to hybridize. The solid lines in this region refer to the bands after hybridization has been taken into account, while the dashed lines refer to the nonhybridized bands. We start the discussion by first considering the band dispersion neglecting hybridization. Clearly the dispersion of the nonhybridized 5σ bands should be similar to the 4σ dispersion. In fact, this is our result. The splittings calculated for various symmetry points, however, differ considerably. This is expected since the spatial extent of the 5σ molecular orbitals is different from the 4σ MOs. This aspect has been discussed in details by Greuter et al. [19]. Compared with the 4σ bands the 5σ bands show a splitting of 1.35 eV at $\overline{\Gamma}$ and 0.63 eV at $\overline{Y}$ since the 5σ MOs are more diffuse than the 4σ MOs.

The dispersion associated with the nonhybridized 1π MO is, due to its twofold degeneracy on the molecular level, slightly more complicated than the σ band dispersions. Since the global symmetry of the adlayer is only twofold the two 1π components cannot be degenerate and, due to the formation of bonding and antibonding combinations, give rise to four bands at $\overline{\Gamma}$. In order to label the bands, we have chosen x to denote the component in [1$\overline{1}$0], y to denote the component in [001] direction. The wavefunctions belonging to the x components are shown in fig. 7b, those belonging to the y component are shown in fig. 7c. Again, bonding and antibonding phase relations are identical to those for the σ bands shown in fig. 7a. Unlike the σ bands, however, the antibonding combination is labelled + and the bonding combination is labelled − in the 1π case. As outlined above, the + or − sign refers to phase factors between unit cells, while bonding and antibonding refers to the character of the wavefunction *within* the unit cell: An in-phase combination of two π functions is antibonding and thus energetically destabilized, the out-of-phase combination of two π functions is bonding and thus energetically stabilized. In other words, π bands associated with phase factors + and − are

energetically reversed with respect to the σ bands. The splitting between $+$ and $-$ bands differs for the x and y components, in agreement with expectations since the lateral interactions along [1$\bar{1}$0] are much stronger than along [001]. The magnitudes of the splitting are 2.1 and 0.78 eV respectively. At $\bar{\Gamma}$, $1\pi_y^-$ and $1\pi_x^+$ belong to the same, while $1\pi_y^+$ and $1\pi_x^-$ belong to different irreducible representations. At $\bar{X}$ the bands degenerate pairwise for the same reason that we used for the σ-bands. The bonding character of the wavefunctions at $\bar{X}$ is clearly higher for the x component than for the y component as is evident from fig. 7b and fig. 7c (left panel). Consequently, the two $1\pi_y$ bands cross with the $1\pi_x^+$ band. Along the $\bar{\Sigma}$ line there are only two irreducible representations. The bands are labelled according to Litvin's compatibility relations [24]. The $1\pi_y^-$ band has the same symmetry as the $1\pi_x^+$ band along $\bar{\Sigma}$, leading to a very small gap around the crossing point. The gap is very small since the interaction is "forbidden" for topological reasons. Perpendicular to the $\bar{\Sigma}$ direction, namely in the $\bar{\Delta}$ direction, the π bands, like the σ bands, are not degenerate at the zone boundary. Along the $\bar{\Sigma}$ direction the two $1\pi_y$ bands cross and, having the same symmetry, are allowed to hybridize. Fig. 7c shows on the right hand side that the $1\pi_y^-$ band is, in addition to its bonding character in [001] direction, also bonding along [1$\bar{1}$0], while $1\pi_y^+$ is bonding along [001], but antibonding along [1$\bar{1}$0]. In that respect, those particular broken lines are without importance, and are not connected with the σ/π hybridization which we shall discuss in the following.

σ/π hybridization can only occur if the bands of π and σ parentage transform according to the same irreducible representations. Obviously, for the $\bar{\Delta}$ direction this is not the case. However, along $\bar{\Gamma}$–$\bar{X}$, i.e. in the $\bar{\sigma}$ direction, the $1\pi_x^-$ band hybridizes with the 5σ band, shifting the energetic position of the point of degeneracy. Note that the degeneracy at $\bar{X}$ is not lifted by σ/π hybridization. However, it is evident that the hybridized band structure is considerably different from the nonhybridized one.

So far we have not discussed the dispersion along $\bar{D}$, $\bar{C}$ and $\bar{\Gamma}$–$\bar{S}$. $\bar{D}$ is the direction in k-space where the bands are forced by symmetry to be degenerate. The energy dispersion along the line is rather small. The x- and y-components are allowed to hybridize along $\bar{D}$, except that there are no forbidden crossings for the $\bar{X}$ and $\bar{S}$ points. On the $\bar{C}$ line the situation is very similar to $\bar{\Sigma}$. The dispersion of the 5σ bands is small enough not to induce σ/π hybridization of any noticeable amount. Along the $\bar{\Gamma} \rightarrow \bar{S}$ direction, symmetry does not restrict the interaction so that all effects noted with respect to the various directions are operative simultaneously.

We conclude the theoretical considerations on the band structure by realizing that the full band structure including effects of the substrate and σ/π hybridization is considerably different from a band structure calculated for a free CO layer.

4. Discussion

Many spectra have been necessary to map out the band structure shown in fig. 8. The dispersion of the bands was determined by recording spectra as a function of the polar angle θ and plotting energy versus $k_{\parallel}$ along two high symmetry lines using the relation

$$k_{\parallel} = \left(2mE_{kin}/\hbar^2\right)^{1/2} \sin \theta.$$

Full dots in fig. 8 indicate the experimental results, whereas the solid lines represent the calculated band structure, which has been shifted such that the energetic position of the $4\sigma^+$ band at $\bar{\Gamma}$ is identical to the experimental one. Note that there is no additional fitting parameter except the tilt angle γ (which was chosen to be 17°) of the CO molecules. There is remarkable agreement between experiment and theory with respect to dispersion and symmetry behaviour: The dispersion of the 4σ bands is described perfectly with respect
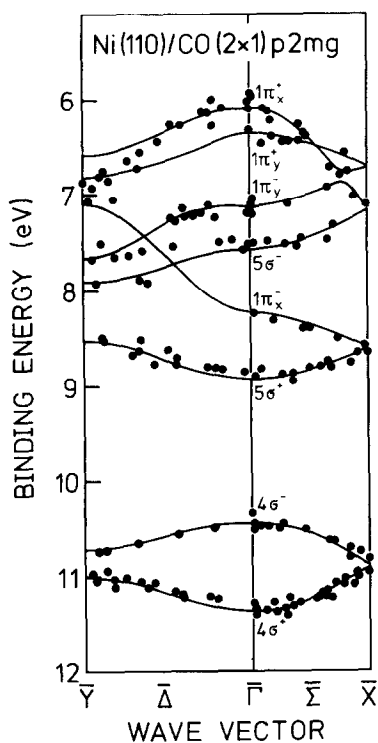

Fig. 8. Comparison of experimental and calculated band structure of a CO (2×1)p2mg structure along $\bar{\Sigma}$ and $\bar{\Delta}$ directions. The labelling refers to theoretical rather than experimental assignments (see text).

Table 1

Dipole selection rules for excitation of photoelectrons in normal direction from a CO (2×1)p2mg adlayer

Electric field vector E		Initial state bands	
Orientation	Symmetry	Molecular assignment	Symmetry
$E \parallel [110]$: z-polarization	Γ_1	$4\sigma^+, 5\sigma^+, 1\pi_y^+$	Γ_1
$E \parallel [001]$: y-polarization	Γ_2	$4\sigma^-, 5\sigma^-, 1\pi_y^+$	Γ_2
–	Γ_3	$1\pi_x^-$	Γ_3
$E \parallel [1\bar{1}0]$: x-polarization	Γ_4	$1\pi_x^+$	Γ_4

Notations are in accordance with those given by Litvin [23,24]. The symmetry of the final state is Γ_1.

to the splitting at $\overline{Y}$ (0.3 eV), the splitting at $\overline{\Gamma}$ (0.8 eV) and the degeneracy at $\overline{X}$. The 4σ dispersion is the largest reported so far [19,25]; of course, the reason is the NiNi distance of only 2.49 Å, which leads to a packing of CO molecules in the (2×1)p2mg phase with the smallest intermolecular separation investigated until now. Also, the symmetry behaviour is correct. At $\overline{\Gamma}$ the symmetry is C_{2v} and the dipole selection rules shown in table 1 can be applied. The final state has to be totally symmetric ($\overline{\Gamma_1}$). From the He II spectra in fig. 3, there is clear evidence for the $\overline{\Gamma_2}$ symmetry of the $4\sigma^-$ band, which can be excited only with y-polarized light. This point is of particular importance since it shows the existence of a mirror plane in [001] direction. Note that the band labels shown in the diagram (fig. 8) refer to theory and not to the experiment. The symmetry restrictions for the $4\sigma^-$ and $4\sigma^+$ bands hold in the same way for the $5\sigma^-$ band with respect to the $5\sigma^+$ band. Applying this procedure we would place the $5\sigma^-$ band experimentally at 7.2 eV binding energy, i.e. the data show a $5\sigma^+/5\sigma^-$ splitting of 1.6 eV. However, our calculation only predicts a splitting of 1.3 eV. While the position of the $5\sigma^+$ levels at $\overline{\Gamma}$ is reproduced correctly the calculated $5\sigma^-$ level binding energy is too large. Even though the relative stabilization of the 5σ-CO derived level with respect to the 1π level is obviously taken into account properly, the intermolecular 5σ interaction is underestimated. We feel that due to the rather good overall agreement between experiment and theory we have basically properly accounted for the direct intermolecular interaction contribution. However, indirect interactions [26] through the metal substrate are not taken into account, which may cause the observed discrepancy. Support is lent to this interpretation by the fact that the calculated 5σ band dispersion, involving an orbital that strongly interacts with the metal, shows a stronger deviation from experiment than the 4σ band dispersion originating from a primarily nonbonding CO–metal level. If we accept the assignment, the (theoretically based) labelling of the 5σ and $1\pi_y^-$ bands at $\overline{\Gamma}$ has to be reversed. This implies, however, that the $1\pi_y$ splitting at $\overline{\Gamma}$ is also calculated too small and is asymmetric with respect to its point of

degeneracy at $\bar{X}$. Again, this could be rationalized by considering interactions of the $1\pi_y$ orbitals with neighbouring metal atoms. This interaction is not taken into account and is only operative for the $1\pi_y$ orbitals, since in this case the tilt along [001] induces a different overlap for the two lobes of the $1\pi_y$ orbital while the $1\pi_x$ lobes experience equal interactions. For these reasons the symmetries $1\pi_y^-$ and $5\sigma^-$ can be exchanged without disturbing the obvious good overall agreement in band dispersions seen in fig. 8. Emission from the $1\pi_x^-$ band is very weak, especially along $\bar{\Delta}$, which again is in agreement with the dipole selection rules. Transitions from the $1\pi_x^-$ band are dipole forbidden in normal emission. Dispersions from the $1\pi_x$ bands are much larger than the dispersions of the $1\pi_y$ bands, indicating a denser packing of CO molecules along the [1$\bar{1}$0] glide line with respect to the [001] direction. From this, we conclude that the strong repulsive interaction of the $1\pi_x$ levels between neighbouring CO molecules leads to the alternating tilt.

In order to arrive at a conclusion about the tilt angle of CO molecules with respect to the surface normal we fitted the band structure calculation to the experimental data by variation of γ. The procedure can be visualized with the help of fig. 9. In the left panel we show the dispersion of the $1\pi_x$ bands as a function of γ. The $1\pi_y$ bands disperse within the hatched area for the
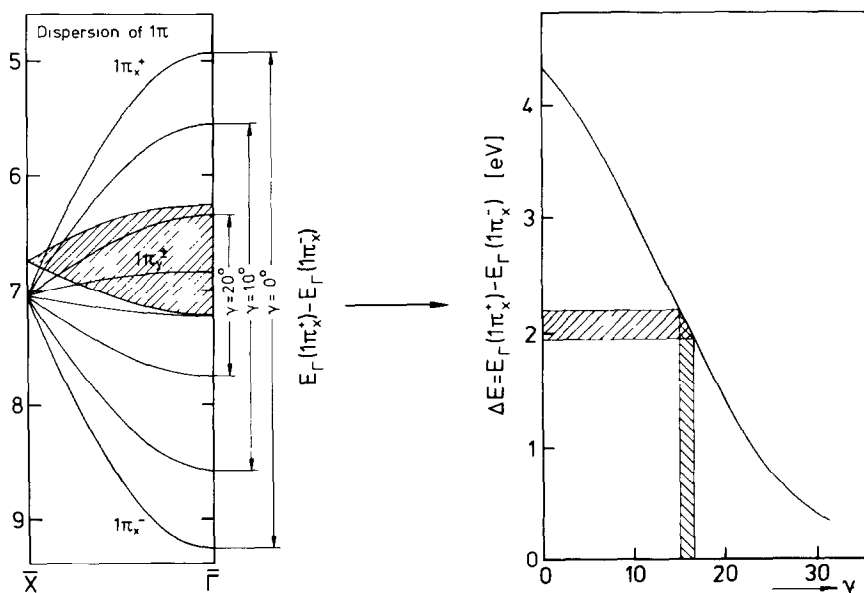
Fig. 9. Schematic band dispersion of the $1\pi_x$ and $1\pi_y$ band systems as a function of tilt angle γ. The hatched area in the left panel covers the comparatively small region of dispersions of the $1\pi_y$ levels. The $1\pi_x$ levels are shown explicitly for four tilt angles. The right panel shows the continuous variation of $1\pi_x$ splitting at $\bar{\Gamma}$ as a function of tilt angle γ. The hatched areas refer to the experimentally observed $1\pi_x$ splitting, which allows the corresponding γ to be estimated.
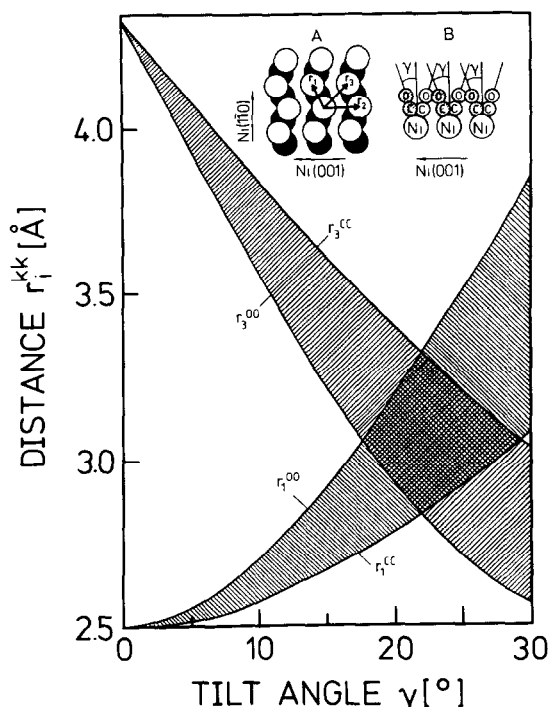
Fig. 10. Interatomic distances r_1, r_2 and r_3 (see insert A) between carbon (superscript CC) and oxygen (superscript OO) atoms as a function of the tilt angle γ.

considered angular variations. We use the $1\pi_x$ bands as an example because for these bands the angular variations are largest so that the fitting procedure is rather precise. For $\gamma = 0°$ the splitting is calculated to be ≈ 4 eV between the band belonging to the bonding and the antibonding combination. Note that for $\gamma = 0°$ the glide plane disappears and we reach a p(1 × 1) structure. In this case the unit cell contains only one molecule, and therefore, instead of having a splitting at $\overline{\Gamma}$ into two bands, the size of the Brillouin zone doubles. However, for comparison we have folded back the bands into a reduced zone, identical to the one for the p2mg structure. Clearly, as soon as we allow the CO molecules to avoid each other by choosing $\gamma > 0°$ the splitting decreases dramatically, until we reach agreement with the experimentally observed splitting of 2.2 eV at $\gamma = 17 \pm 2°$. This is graphically shown in the panel on the right hand side of fig. 9. This strong variation of the 1π splitting is a consequence of the strong variation of intermolecular distances as a function of γ. Fig. 10 shows the variations of various interatomic distances within the two-dimensional layer versus tilt angle γ. The nomenclature is explained in the inserts. CC refers to carbon–carbon, OO to oxygen–oxygen distances. The

hatched areas cover the regions of intermolecular distances between CO molecules. In [1$\bar{1}$0] direction the distance increases as a function of γ, with a more rapid increase for r_1^{OO} than for r_1^{CC}. However, the separation r_3 decreases at the same time, even more rapidly as γ increases. Obviously, the interplay between decreasing lateral interaction along r_1 and increasing lateral interaction along r_3 limits the tilt angle γ. Usually, it is assumed that the intermolecular distance is ≈ 3 Å. For the oxygen–oxygen interaction this limit is reached at the intersection point around $\gamma = 18°$. At this point the carbon–carbon separation is only 2.7–2.8 Å. It is not unreasonable to assume that the carbon in fact uses not as much space as the oxygen when CO is chemisorbed. This in turn, would allow for a shorter carbon–carbon separation. On the other hand, a slight deviation from a linear metal–CO bond would lead to a larger C–C separation. Bending the CO–metal bond by 5° at the carbon atom increases the C–C separation by 5% or 0.15 Å along [1$\bar{1}$0], resulting in a value close to ≈ 3 Å. From this simple geometric argument one already gets a result consistent with the band structure fit.

5. Conclusions

We have presented a detailed photoemission study for the system CO/Ni(110) at $\theta = 1.0$. Our results, in particular polarization dependent intensity variations of the CO induced emission, clearly show the existence of a mirror plane along [001] in addition to the [1$\bar{1}$0] glide plane. Thus, our results support the proposal that the structure has p2mg symmetry, as opposed to p1g1 symmetry in agreement with the corresponding results on Pt(110) (question (i) in the introduction). Stepping further to question (ii) asked in the introduction we refer to fig. 11. Here, all presently available 4σ band widths have been plotted as a function of the intermolecular separation (R) assuming a simple exponential dependence of the band width on R. Such a dependence must be expected if the band width is determined by wavefunction overlap as was pointed out by Greuter et al. [19]. Clearly the present value correlates very nicely with literature data but represents the largest value reported so far.

We have shown (question (iii)) that the observed band structure can be well reproduced by tight-binding calculations of an unsupported CO overlayer of p2mg symmetry if the interaction with the substrate is included so as to account for 4σ–5σ mixing upon chemisorption as well as the 5σ–1π hybridization caused for the energetic proximity of the 5σ and 1π levels. However, certain deviations between experiment and theory allow us to deduce information about the possible influence of indirect intermolecular interactions within the adlayer. Finally, the rather large splitting at $\bar{\Gamma}$ within the manifold of 1π derived levels, in particular the splitting of the $1\pi_x$ components along the glide plane [1$\bar{1}$0], allow us to estimate the tilt angle of the CO–metal bond to be
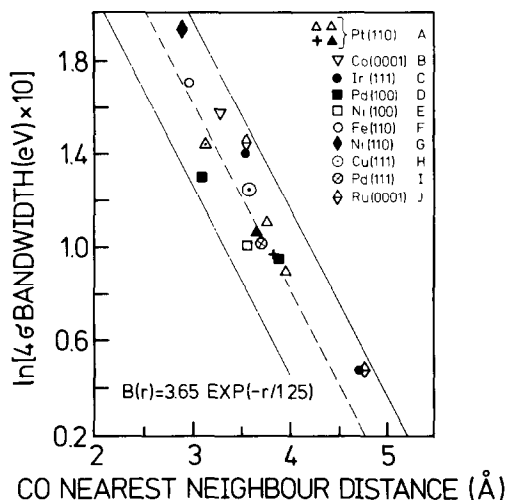
Fig. 11. CO 4σ band width as a function of CO nearest neighbour distances for various substrates (see ref. [27]). CO band widths have been corrected for those structures which are not hexagonal (see ref. [19]).

$17 \pm 2°$ in agreement with Riedl and Menzel's [2] ESD results. Very recent bremsstrahlung isochromat spectra [28] for the same system reveal correspondingly strong intermolecular interactions within the manifold of unoccupied CO-2π derived levels. The magnitude of the intermolecular interaction on the unoccupied levels is compatible with estimates from calculations that use the structural information based on the present study.

Acknowledgements

References

[1] R.J. Behm, G. Ertl and V. Penka, Surface Sci. 160 (1985) 387.
[2] W. Riedl and D. Menzel, Surface Sci. 163 (1985) 39.
[3] D. Rieger, R.D. Schnell and W. Steinmann, Surface Sci. 143 (1984) 157.
[4] P. Hofmann, S.R. Bare and D.A. King, Surface Sci. 117 (1982) 245;
    P. Hofmann, S.R. Bare, N.V. Richardson and D.A. King, Solid State Commun. 42 (1982) 645.

[5] R.S. Bare, K. Griffiths, P. Hofmann, D.A. King, G.L. Nyberg and N.V. Richardson, Surface Sci. 120 (1982) 367.

[6] B.J. Bandy, N.A. Chesters, P. Hollins, J. Pritchard and N. Sheppard, J. Mol. Struct. 80 (1982) 203.

[7] P.R. Mahaffy and M.J. Dignam, Surface Sci. 97 (1980) 377.

[8] J.C. Bertolini and B. Tardy, Surface Sci. 102 (1981) 131.

[9] M. Nishijima, S. Masuda, Y. Sakisaka and M. Onchi, Surface Sci. 107 (1981) 31.

[10] J. Lee, J. Arias, C. Hanrahan, R. Martin, H. Metiu. C. Klauber, M.D. Alvey and J.T. Yates, Jr., Surface Sci. 159 (1985) L460.

[11] R.M. Lambert, Surface Sci. 49 (1985) 325;
     B.W. Holland and D.P. Woodruff, Surface Sci. 36 (1973) 488.

[12] H. Kuhlenbeck, M. Neumann and H.-J. Freund, to be published.

[13] W. Eberhardt and E.W. Plummer, Phys. Rev. B21 (1980) 3245;
     R. Clauberg, W. Gudat, W. Radlik and W. Braun, Phys. Rev. B31 (1985) 1754.

[14] E.W. Plummer, T. Gustafson, W. Gudat and D.E. Eastman, Phys. Rev. A15 (1977) 2339.

[15] J.W. Davenport, Phys. Rev. Letters 36 (1976) 945;
     C.L. Allyn, T. Gustafson and E.W. Plummer, Chem. Phys. Letters 47 (1977) 127.

[16] H. Jones, Theory of Brillouin Zones (North-Holland, Amsterdam, 1975).

[17] J. Callaway, Quantum Theory of the Solid State (Academic Press, New York, 1974);
     B.J. Ransil, Rev. Mod. Phys. 32 (1960) 245.

[18] J.A. Pople and D.L. Beveridge, Approximate Molecular Orbital Theory (McGraw-Hill, New York, 1970).

[19] F. Greuter, D. Heskett, E.W. Plummer and H.-J. Freund, Phys. Rev. B27 (1983) 7117.

[20] For one of the early band structure calculations on a free unsupported CO overlayer, see, e.g., K. Horn, A.M. Bradshaw, K. Hermann and I.P. Batra, Solid State Commun. 31 (1979) 257.

[21] Use of bridged Ni_2CO clusters would result in minor differences.

[22] F. Hund, Z. Phys. 99 (1936) 119.

[23] D.B. Litvin, Thin Solid Films 106 (1983) 203.

[24] D.B. Litvin, J. Phys. C17 (1984) L37.

[25] D. Rieger, PhD Thesis, Universität München (1984).

[26] J. Koutecky, Trans. Faraday Soc. 54 (1958) 1038;
     T.B. Grimley, Advan. Catalysis 12 (1960) 1;
     T.L. Einstein and J.R. Schrieffer, Phys. Rev. 137 (1973) 3629.

[27] (A) cf. refs. [3,25].
     (B) cf. ref. [10];
     (C) C.W. Seabury, E.S. Jensen and T.N. Rhodin, Solid State Commun. 37 (1981) 383;
     (D) K. Horn, A.M. Bradshaw, K. Hermann and I.P. Batra, Solid State Commun. 31 (1979) 257;
     (E) K. Horn, A.M. Bradshaw and K. Jacobi, Surface Sci. 72 (1978) 719;
     (F) E.S. Jensen and T.N. Rhodin, Phys. B27 (1983) 3338;
     (G) this work;
     (H) H.-J. Freund, W. Eberhardt, D. Heskett and E.W. Plummer, Phys. Rev. Letters 50 (1983) 768;
     (I) R. Miranda, K. Wandelt, D. Rieger and R.D. Schnell, Surface Sci. 139 (1984) 257;
     (J) (a) P. Hofmann, J. Gossler, A. Zartner, M. Glanz and D. Menzel. Surface Sci. 161 (1985) 303;
         (b) D. Heskett, E.W. Plummer, R.A. de Paola, W. Eberhardt and F.M. Hoffmann, Surface Sci. 164 (1985) 490.

[28] J. Rogozik, V. Dose, M. Neumann and H.-J. Freund, Surface Sci., submitted.